AIAA JOURNAL
Vol. 43, No. 11, November 2005

Passive Control for Turbofan Tonal Noise

B. Elhadidi* and H. M. Atassi†
University of Notre Dame, Notre Dame, Indiana 46556

A three-dimensional linearized Euler model is developed for the interaction and scattering of unsteady incident disturbances by an annular cascade of unloaded blades. The model is first used to examine the validity of the popular two-dimensional strip theory for three-dimensional annular cascades at frequencies relevant to fan engine noise. It is then applied to investigate three methods of passive control for turbofan tonal noise, namely, blade lean, blade sweep, and mean flow acceleration. Because blade lean and sweep generally enhance the blade upwash radial phase variation, an analysis is carried out to examine the effects of the radial modulation of the incident disturbances on the annular cascade sectional lift and the modal acoustic response. Noise control by blade lean and sweep is then investigated for typical fans. The results show that blade lean or sweep can be designed to be effective noise reduction mechanisms; however, their effectiveness depends on the characteristics of the incident disturbances and the number of propagating duct modes. Converging ducts are also shown to be effective sound reduction mechanisms.

Nomenclature

B = number of rotor blades
c = chord length, m
$c_{l'}$ = unsteady sectional lift coefficient
c_{mn} = sound pressure amplitude
c_0 = speed of sound, m/s
$\boldsymbol{e}$ = direction vector
k = axial wave number, 1/m
L = computational domain length, m
M = axial Mach number
$\mathcal{M}$ = mapping function
m = azimuthal mode number
N = number of grid points
$\boldsymbol{n}$ = normal direction
P = sound power, W
$\mathcal{P}$ = pressure eigenmode
p = pressure, Pa
r = radial coordinate, m
S = permissible set of solutions for eigenfunction expansion
t = time, s
$\boldsymbol{U}$ = velocity, m/s
$\boldsymbol{u}$ = unsteady velocity, m/s
V = number of stator vanes
x = axial position, m
α = sweep angle, deg
β = lean angle, deg
θ = azimuthal angle, deg
ϑ = angular spacing, deg
Λ = convected eigenvalue
ξ = transformed distance, m
ρ = density, kg/m^3
σ = interblade phase angle
ϕ = potential, m^2/s
Ω = shaft rotational speed, rad/s
ω = gust angular frequency, rad/s

Subscripts

h = evaluated at hub radius
I = evaluated at inlet of computational domain
in = quantities at inflow
m = acoustic azimuthal mode number
m = evaluated at mean radius
m_g = upstream disturbance azimuthal mode number
n = acoustic radial mode number
n_g = upstream disturbance radial mode number
out = quantities at outflow
r = radial direction
t = evaluated at tip radius
x = axial direction
θ = azimuthal direction
0 = steady flow quantity

Superscripts

R = vortical velocity
$'$ = perturbation
$\tilde{()}$ = nondimensional quantity
$\bar{()}$ = complex conjugate
$\pm$ = downstream (+) and upstream (−) direction

Introduction

ENGINE noise at approach and takeoff is one of the most critical components of total aircraft noise. For modern-day large bypass turbofan engines, one of the major noise components is that generated by the interaction of rotor wake with the stator vanes, which is known as fan interaction noise. Future turbofan engines will be designed with larger bypass ratios in which fan noise becomes even more significant compared to the total engine noise,[1,2] as qualitatively shown in Fig. 1. There are two major noise-reduction techniques: active and passive. Active suppression, such as boundary-layer suction and fan wake management, techniques[3] have been successful; however, they imply delicate and expensive control systems. Passive suppression techniques are relatively simpler to implement because they are incorporated in the fan design and require less maintenance than active suppression techniques.

Currently passive noise-reduction techniques rely on design experience. The efficiency of a passive noise-reduction technique depends on both the number and the amplitude of the propagating duct modes. Thus, the radiated sound power can be reduced by three major techniques: 1) reducing the number of propagating duct modes, 2) attenuating the amplitude of the propagating duct modes, and/or 3) changing the amplitude of the propagating duct modes.

The number of propagating duct modes can be reduced by use of convergent-divergent ducts because ducts with small tip/hub ratios

Received 18 December 2003; revision received 12 July 2004; accepted for publication 28 February 2005.

*Research Associate, Department of Aerospace and Mechanical Engineering.
†Viola D. Hank Professor, Department of Aerospace and Mechanical Engineering. Fellow AIAA.

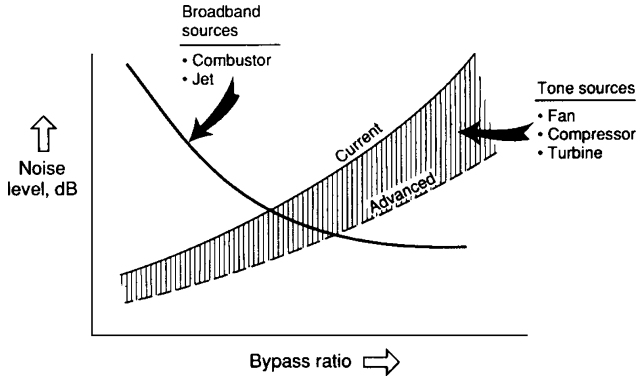

Fig. 1 Qualitative trends for engine noise sources.[1]

have less propagating duct modes than ducts with large tip/hub ratios. Another way for reducing the number of propagating modes is to eliminate certain modes by modifying the number of rotor and stator blades. Tyler and Sofrin[4] showed that the propagating duct modes for the first blade harmonic can be cut off if the number of rotor blades and stator vanes are chosen correctly. Recently Elliot and Dittmar[5] modified the number of rotor blades and stator vanes so that the perceived noise levels are beyond the audible frequency range. This, however, requires a large number of rotor blades and is not technologically feasible for production at the moment.

Duct liners can be used to reduce noise by attenuating the amplitude of the propagating duct modes. However, duct splices used to connect the liners together increase the number of attenuated propagating duct modes. This can significantly reduce the liner efficiency.[6] Furthermore, the benefits of liners will likely diminish as the engine bypass ratio is increased because increasing the bypass ratio is usually effected with a reduction of the nacelle thickness, hence a reduction in the liner depth, which leads to a reduction of liner effectiveness.[2]

Sound reduction by modifying the amplitude of the propagating duct modes can be obtained by modifying the unsteady vane loading. This can be achieved by extending the rotor/stator spacing or by implementing stator vane lean and/or sweep. Experimental evidence suggests that increased rotor/stator spacing is an effective noise-reduction mechanism.[1,7] However, the excess engine weight penalty and additional external aerodynamic drag can affect the overall reduction gains. In these experiments the sound reduction was attributed to the viscous decay of the rotor wake; however, the authors showed[8] that the reduction is mainly caused by the modified unsteady vane loading generated by mean flow swirl. Moreover, increasing the rotor/stator spacing will result in noise reduction only if the swirling mean flow is hydrodynamically stable. Experimental evidence also suggests that vane lean and sweep (Fig. 2) can produce significant reductions for fan noise over a wide range of operating conditions.[9,10] The experiments show that the sound power reduction is not caused by the viscous wake decay as the rotor/stator spacing is increased for the swept vane. Rather the sound power reduction is caused by the modification of the radial phase of the incoming gust as it interacts with the swept vane. Traditionally, the vanes are swept back, as a means to increase the rotor/stator spacing. More recently, forward rotor-blade sweep has been experimentally examined as a means for noise reduction.[11] However, the reduction sought by increased rotor/stator spacing was not observed in these experiments.

Previously, theoretical studies have examined the unsteady response caused by incident rotor wakes interacting with swept and/or leaned vanes. Schulten[12,13] applied a lifting surface formulation, whereas Envia and Nallasamy[10] applied a strip theory approach, which was coupled to a duct propagation code. Schulten[12] concluded that lean is not effective, whereas Envia and Nallasamy[10] demonstrated that lean is effective, if applied in the direction of fan rotation. Also, Schulten[13] predicted that vane sweep for high Mach numbers is only effective for large sweep angles, whereas Envia and Nallasamy[10] concluded that positive sweep will always be effective.

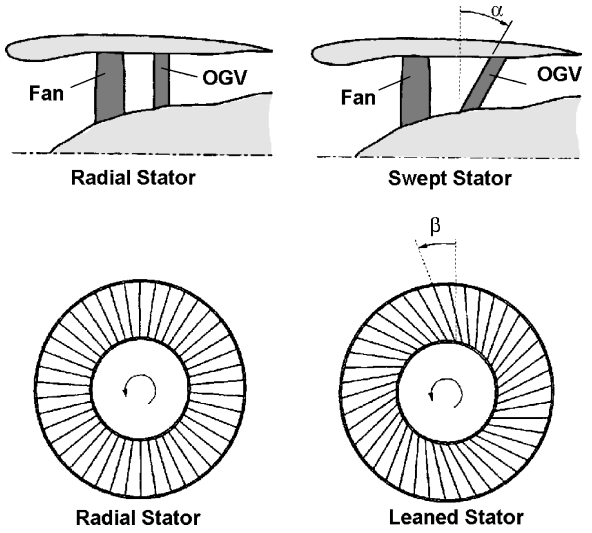

Fig. 2 Schematic comparing a) vane sweep and b) vane lean.[10]

In this paper we investigate noise reduction by stator vane lean or sweep for the case of a constant uniform axial mean flow. We first develop a three-dimensional linearized Euler analysis, and we reexamine the numerical results of Schulten[12,13] and Envia and Nallasamy.[10] We then apply the numerical model to resolve the differing conclusions between these two models. We also examine the validity of the strip theory approach and show the requirement for full three-dimensional calculations. Second, we investigate lean and sweep independently from one another to establish benchmark results and to examine the efficiency of each technique. In doing so we examine a variety of test cases to determine the conditions for which lean or sweep are effective. We also investigate the efficiency of nontraditional techniques such as forward-swept vanes. Third, we investigate the benefits of using convergent annular ducts to reduce the radiated sound power.

We begin by formulating the problem and presenting the governing equations. Results are presented to demonstrate the need for three-dimensional calculations compared to a strip theory approach. We then examine how radial phase variations for the incident gusts excite different propagating acoustic modes. Finally, we apply our formulation to various noise-reduction mechanisms and present conclusions.

Formulation

For simplicity, we consider an annular cascade of unloaded blades at zero stagger. We model the flow using the linearized Euler equations. With these assumptions the computational domain can be reduced to a single vane passage extended upstream and downstream along the streamlines as shown in Fig. 3. We complete our formulation by developing the initial and boundary conditions along the computational domain. We end this section by developing all of the postprocessing tools needed to examine the efficiency of a noise-reduction mechanism.

Governing Equations

The flow variables, velocity $\boldsymbol{U}$, pressure p, and density ρ are considered to be the sum of their mean values $\boldsymbol{U}_0$, p_0, and ρ_0 and their disturbances $\boldsymbol{u}$, p', and ρ'. We use the cylindrical coordinates (x, r, θ), where x is along the machine axis. For the blade geometry considered, we assume the mean flow to be isentropic and potential of the form

$$\boldsymbol{U}_0(x, r) = U_x(x, r)\boldsymbol{e}_x + U_r(x, r)\boldsymbol{e}_r \tag{1}$$

where U_x, U_r are the axial and radial mean flow components, respectively, and $\boldsymbol{e}_x$, $\boldsymbol{e}_r$ are unit vectors in the axial and radial directions. For the cases involving vane lean and sweep, the mean flow is constant and uniform and of the form, $\boldsymbol{U}_0 = U_x\boldsymbol{e}_x$. For the case of a

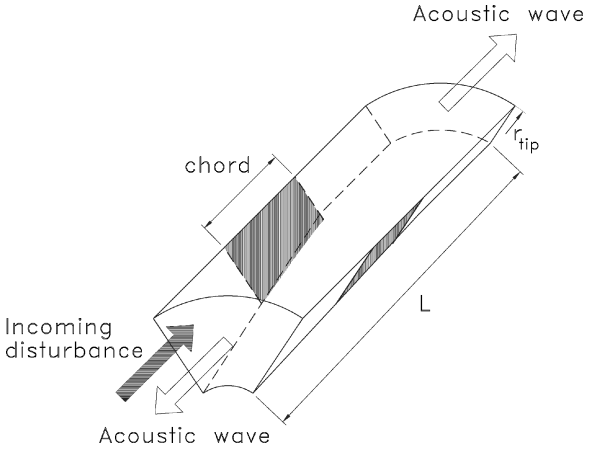

Fig. 3 Schematic of the computational domain.

converging annular duct, the duct cross section is chosen to be uniform at the duct inlet and exit so that the mean flow at inflow and outflow is constant and uniform. This is an important assumption in this work because the nonreflecting boundary conditions are only developed for nonaccelerating mean flows.

It is convenient to represent the unsteady velocity disturbance as the sum of a vortical component $\boldsymbol{u}^{(R)}$ and an irrotational component $\nabla\phi$:

$$\boldsymbol{u}(\boldsymbol{x}, t) = \boldsymbol{u}^{(R)} + \nabla\phi \tag{2}$$

For irrotational mean flow the governing equations reduce to[14,15]

$$\frac{\mathrm{D}_0\boldsymbol{u}^{(R)}}{\mathrm{D}t} + \boldsymbol{u}^{(R)} \cdot \nabla \boldsymbol{U}_0 = 0 \tag{3}$$

$$\frac{\mathrm{D}_0}{\mathrm{D}t}\left(\frac{1}{c_0^2}\frac{\mathrm{D}_0\phi}{\mathrm{D}t}\right) - \frac{1}{\rho_0}\nabla\cdot(\rho_0\nabla\phi) = \frac{1}{\rho_0}\nabla\cdot\left(\rho_0\boldsymbol{u}^{(R)}\right) \tag{4}$$

where c_0 is the mean flow speed of sound and $\mathrm{D}_0/\mathrm{D}t = \partial/\partial t + \boldsymbol{U}_0\cdot\nabla$ is the material derivative associated with the mean flow. The pressure is given by

$$p' = -\rho_0\frac{\mathrm{D}_0\phi}{\mathrm{D}t} \tag{5}$$

We consider a single frequency component and take $\{\boldsymbol{u}^{(R)}, \phi\} = \{\tilde{\boldsymbol{u}}^{(R)}, \tilde{\phi}\}e^{-i\omega t}$.

In the frequency domain, Eq. (3) reduces to first-order ordinary differential equations along the mean flow streamlines, and its solution requires only initial conditions at the inlet of the computational domain. Equation (4) is, however, elliptic in the frequency domain, and its solution requires boundary conditions along the duct, blades, and free surfaces upstream and downstream of the blades, and nonreflecting conditions at the inflow/outflow surfaces of the computational domain. To simplify the application of these conditions, we use the mean flow streamlines as one of the coordinates in the numerical solution of Eqs. (3) and (4).

Initial Conditions

The single vane passage is bounded by two stream surfaces as shown in Fig. 3. At x_I, the axial position of the computational domain inlet, we apply initial conditions for Eq. (3). Without loss of generality, an incoming vortical gust can be represented in terms of its Fourier components as

$$\boldsymbol{u}^{(R)}(x_I, r, \theta, t) = \sum_{m_g=-\infty}^{\infty} \boldsymbol{a}_{m_g}(r)\exp[i(k_x x_I + m_g\theta - \omega t)] \tag{6}$$

where m_g is the azimuthal mode number for the vortical disturbance, $\boldsymbol{a}_{m_g} = \{a_{m_g x}, a_{m_g r}, a_{m_g\theta}\}$ is the amplitude vector of the gust Fourier mode, and $k_x = \omega/U_{x(\mathrm{in})}$ is the axial wave number, where $U_{x(\mathrm{in})}$ is the constant axial mean flow at inflow. The phase $k_x x_I$ is included in the right-hand side of Eq. (6) to account for the variable axial location of the computational domain for the problem of vane sweep. For tonal noise calculations, we consider harmonic disturbances with a frequency $\omega = m_g\Omega$, where Ω is the shaft angular velocity. The gust azimuthal mode number is given by $m_g = pB$, where B is the number of upstream rotor blades and p is an integer that represents the order of the blade passing frequency (BPF). For this study we only consider the first BPF, that is, $p = 1$. At incidence, the duct cross section is constant, and the mean flow is uniform. As a result, the incident vortical disturbance is solenoidal.[15] It is convenient to expand the radial variation of the incident disturbance in Fourier modes and to consider the cascade response to a single Fourier component. For simplicity, we further neglect the radial component of the disturbance velocity and assume the incident vortical disturbance to be of the form

$$\boldsymbol{a}_{m_g} = (-m_g U_x/r\omega, 0, 1)a_{m_g\theta}\exp\{i\pi n_g[(r - r_h)/(r_t - r_h)]\} \tag{7}$$

where $a_{m_g\theta}$ is a constant and n_g is an integer that characterizes the upwash spanwise phase variation. With this representation, the variation in the radial profile of the incident gust is accounted for as variation in the radial phase of the incident gust. Note that n_g indicates the number of zero crossings of the real part of $\boldsymbol{a}_{m_g}$. As the rotor wakes propagate, they appear distorted and bent in the azimuthal direction with respect to the the vanes' leading edges by flow swirl and/or by the vane lean and sweep. This is commonly referred to as the wake intersecting the vane. In the present study, the parameter n_g characterizes the vane upwash radial profile modification caused by the rotor wakes' distortion. Hence, if an incident disturbance is dominated by a certain n_g component, it is an indication of the number of intersections of the wake with the vane.

For nonswirling mean flows, as considered in this paper, the vane upwash is defined as the unsteady normal velocity to the vane surface:

$$a_{m_g\theta}\exp\{i\pi n_g[(r - r_h)/(r_t - r_h)]\}\cos\beta \tag{8}$$

where β is the blade lean angle as shown in Fig. 2 and r_t, r_h are the tip and hub radii, respectively.

Boundary Conditions

Three types of boundary conditions are imposed for Eq. (4) in the computational domain shown in Fig. 3. At the hub and tip radii and vane surfaces we have solid surfaces, along which we apply the impermeability conditions

$$\boldsymbol{u}\cdot\boldsymbol{n} = 0 \tag{9}$$

where $\boldsymbol{n}$ is the unit vector normal to the solid surfaces. Along the free surfaces (upstream and downstream of vane section), we impose continuity of the normal velocity and pressure. These continuity conditions are transformed into quasi-periodicity conditions for the pressure and the normal velocity when applied along free surfaces bounding the computational domain:

$$p'(x, r, \vartheta) = p'(x, r, 0)e^{i\sigma} \tag{10}$$

$$\boldsymbol{u}\cdot\boldsymbol{n}(x, r, \vartheta) = \boldsymbol{u}\cdot\boldsymbol{n}(x, r, 0)e^{i\sigma} \tag{11}$$

Here $\vartheta = 2\pi/V$ is the angular vane spacing, $\sigma = 2pB\pi/V$ is the interblade phase angle, and $\boldsymbol{n}$ is the unit vector normal to the stream surface. Because Eq. (10) expresses the pressure continuity along the wake starting from the trailing edge, it also implies the application of the Kutta condition at the trailing edge.

At the inflow and outflow boundaries, the following nonreflecting boundary conditions are implemented. We seek a relationship between the values of p' at an outgoing (incoming) section x_1 to those inside the numerical domain x_2 of the form

$$p'(x_1, r, \theta) = \mathcal{M}p'(x_2, r, \theta) \tag{12}$$

Golubev and Atassi[16] and Atassi et al.[17] developed this mapping for three-dimensional flows. In their formulations a collocation technique was applied to obtain the mapping function. The collocation technique needs a matrix inversion, which in many cases is difficult because the matrix is ill conditioned. Here, we applied a technique tested and developed by Elhadidi,[8] which does not need any matrix inversion process and is suitable for problems with vane lean or sweep and high-frequency calculations.

Numerical Procedure

For the case of a nonuniform flow, we first solve the steady nonlinear Euler equations to calculate the mean-flow velocities and determine the mean-flow streamlines. The computational grid for the unsteady flow uses the mean-flow streamlines as coordinates. This reduces Eq. (3) to an ordinary set of differential equations in the frequency domain. In the present work we integrate these equations using a fourth-order Runge–Kutta integrator. Then we solve the harmonic wave equation (4) using a second-order central finite difference scheme. The resulting algebraic system of equations is solved using a PETSc[18] package, which is based on an iterative biconjugate gradient stabilized technique and incomplete lower–upper (ILU) factorization.

The model is computationally efficient, and results for a single frequency can be obtained in minutes on a single-processor SunBlade 1000 computer. Extensive code convergence tests and validation with the benchmark aeroacoustic rotor/stator interaction problem proposed by Hanson[19] have been carried out by Elhadidi.[8]

Normalization and Data Processing

At inflow, the mean-flow quantities are uniform and constant. Hence we normalize the mean-flow velocity and density with respect to $c_{0(\mathrm{in})}$ and $\rho_{0(\mathrm{in})}$, where $c_{0(\mathrm{in})}$ is the speed of sound at inflow, and $\rho_{0(\mathrm{in})}$ is the mean-flow density at inflow. All length scales are normalized with respect to the mean radius r_m calculated at inflow. The unsteady pressure p' is normalized with respect to $\rho_{0(\mathrm{in})}c_{0(\mathrm{in})}|a_{m_g\theta}\cos\beta|$. The reduced frequency $\tilde{\omega}$ is normalized with respect to the mean radius and the speed of sound $\tilde{\omega}=\omega r_m/c_{0(\mathrm{in})}$. The sectional unsteady lift coefficient $c_{l'}$ is defined as

$$c_{l'}=\frac{1}{\rho_{0(\mathrm{in})}c_{0(\mathrm{in})}\left|a_{m_g\theta\cos\beta}\right|c}\int_0^c \Delta p'\,\mathrm{d}\xi \tag{13}$$

where ξ is the coordinate along the blade chord c.

To calculate the acoustic power, we first need to express the outgoing unsteady pressure in terms of the propagating pressure eigenmodes, which represent the unsteady pressure in the far field[17]:

$$p'(\boldsymbol{x})=\sum_{m,n\,\in\,S_{\mathrm{mn}}} c^{\pm}_{\mathrm{mn}}\mathcal{P}^{\pm}_{\mathrm{mn}}(r)\exp\left[i\left(k^{\pm}_{\mathrm{mn}}x+m\theta\right)\right] \tag{14}$$

where m and n are the azimuthal and radial mode numbers for the acoustic modes. S_{mn} is the set of all values of m and n for the propagating modes, where m is determined from the Tyler–Sofrin[4] condition for tonal noise calculations ($m=pB\pm qV$, where q is an integer) and n is the radial mode number for a given azimuthal mode m. The k_{mn} and $\mathcal{P}_{\mathrm{mn}}$ are the axial eigenvalue and the corresponding eigenfunction (mode) mn. $\mathcal{P}_{\mathrm{mn}}$ is normalized so that its maximum is equal to unity, and the coefficient c_{mn} represents the magnitude of the unsteady pressure for the mode mn.

To express the efficiency of noise reduction, we calculate the relative acoustic power change (RAPC) to the case of zero lean, sweep, and constant duct radii:

$$\mathrm{RAPC}=100\times(P-P_{\alpha=\beta=0})/P_{\alpha=\beta=0} \tag{15}$$

where $P_{\alpha=\beta=0}$ is the acoustic power at zero lean and sweep. The RAPC can be related to the more common decibel scale:

$$\Delta P_{\mathrm{db}}=10\log\left(P/P_{\alpha=\beta=0}\right)=10\log(1+\mathrm{RAPC}/100) \tag{16}$$

The average acoustic sound power P_{mn} can be calculated for a uniform flow from the expression for acoustic intensity:

$$I_{\mathrm{xmn}}=\left(p'_{\mathrm{mn}}/\rho_0+U_x u_{\mathrm{xmn}}\right)\left[\rho_0 u_{\mathrm{xmn}}+U_x\left(p'_{\mathrm{mn}}/c_0^2\right)\right] \tag{17}$$

where p'_{mn} and u_{xmn} stand for the acoustic pressure and axial velocity for the mode mn. Integrating over the duct cross section, using the orthogonality of the modes, and taking the time average yields the average acoustic power:

$$P=\sum_{\mathrm{mn}=\,\in S_{\mathrm{mn}}}\pi\frac{\omega k_{\mathrm{mn}}}{\rho_0\Lambda^2_{\mathrm{mn}}}\left(1-\frac{U_x}{c_0^2}\frac{\Lambda_{\mathrm{mn}}}{k_{\mathrm{mn}}}\right)|c_{\mathrm{mn}}|^2\int_{r_h}^{r_t}\mathcal{P}_{\mathrm{mn}}(r)\overline{\mathcal{P}_{\mathrm{mn}}(r)}r\,\mathrm{d}r \tag{18}$$

where $\Lambda_{\mathrm{mn}}=-\omega+U_x k_{\mathrm{mn}}$ is the eigenvalue associated with the convective material derivative. The expression for acoustic power in Eq. (18) is only valid for the case of axial uniform flow at the outflow and inflow sections. Designs that efficiently reduce the radiating sound power should have a negative RAPC.

Results

We investigate various noise-reduction mechanisms in this section. First we validate the numerical code and examine the validity of the strip theory and the requirement for three-dimensional calculations. An essential feature of strip theory is the use of two-dimensional models to calculate the unsteady vane loading. For two-dimensional mean flows the radial modulation of the incoming gust (7) can be factored out because the scattered field has exactly the same behavior.[15] For three-dimensional flows, this is not the case. The gust radial variation can be chosen arbitrarily; however, the radial variation of the scattered field is determined by the shape of the duct acoustic modes. The different radial variations between the incident gust and the scattered field strongly affect both the unsteady pressure along the vane and the intensity of the scattered field, that is, the radiated acoustic response. In what follows, this effect will be examined for three test cases. From these studies, we then analyze the mechanism of sound reduction by vane lean, sweep, or by using vanes in converging annular ducts. Unless otherwise stated, we calculate the unsteady response for a fan with a tip/hub ratio $r_t/r_h=2$. The solidity at the tip is equal to unity, and the chord $c=2\pi r_t/V$ is constant along the span. The computational domain length is $L=3c$, where we set one chord length both upstream and downstream of the vane row. We set the origin of the x axis at the hub inlet section, that is, $x_1=0$ at $r=r_h$; hence, the leading edge is at $x=c$. Here we take the number of rotor blades $B=16$, that of the stator vanes $V=24$, and the axial Mach number $M_x=0.5$. This geometry is identical to the geometry of the benchmark aeroacoustic test problem for rotor/stator interaction noise.[19] Hence we refer to it as the benchmark case. For all computations, the number of grid points in the x, r, and θ directions are, respectively, $N_x=181$, $N_r=41$, and $N_\theta=31$.

Code Validation

To validate our results, we consider the computational aeroacoustics (CAA) benchmark rotor/stator interaction problem proposed by Hanson[19] for uniform mean flow and compare our numerical solutions with those of Namba and Schulten based on the lifting-surface model and reported by Schulten and Namba.[20] The downstream acoustic pressure amplitudes ($|c^+_{-8,0}|$ and $|c^+_{-8,1}|$) are shown in Fig. 4 for different n_g. The agreement between our computational solutions and those of Schulten is excellent. We will also compare the unsteady pressure distribution along the blade chord with the results from Schulten in the following section.

Three-Dimensional Calculations vs Strip Theory

A popular approach to internal three-dimensional flows is the strip theory wherein the three-dimensional annulus is considered as a superposition of several narrow annuli. This approximation is commonly used to compute the steady mean flow for lightly loaded vanes.[21] Several investigators have extended the strip theory approach to calculate the unsteady aerodynamic vane response and the

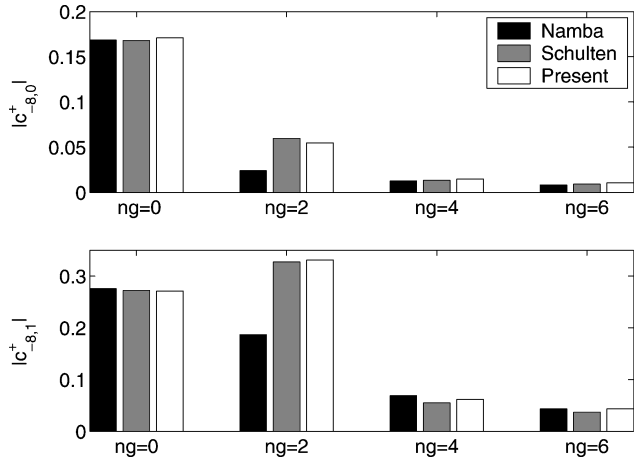

Fig. 4 Comparison of the downstream acoustic pressure amplitudes for benchmark CAA test problem with $M_x = 0.5$, $\tilde{\omega} = 3\pi$, $r_t/r_h = 2$. Figures compare the absolute components of the acoustic pressure for different n_g with those calculated by Namba and Schulten.

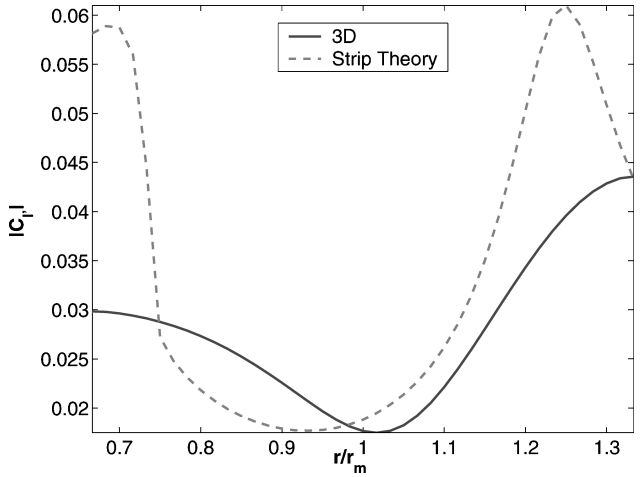

Fig. 5 Comparison of the amplitude of the sectional lift coefficient computed using a three-dimensional model and a strip theory approach: $\tilde{\omega} = 3\pi$, $M_x = 0.5$, $r_t/r_h = 2$, $B = 16$, $V = 24$, $n_g = 0$, and $\alpha = \beta = 0$.

radiated sound pressure.[10] First the unsteady pressure distribution along each narrow annulus is computed from an integral equation-based code such as LINC.[22] The pressure distribution along the vane surface is then used to compute the radiated sound in a duct using a Green's function formulation.

Majumdar and Peake[23] and Elhadidi[8] have examined the validity of the strip theory for a duct. They have concluded that the strip theory can produce reasonable results, for low Mach numbers and low frequencies, such that the number of propagating modes in the duct is equal to the number of cut-on modes in each strip. There are two issues associated with the strip theory when applied to internal aerodynamics with sound propagation. First, the number of propagating modes can vary from one strip to another as we move along the span. Second, as already mentioned, the strip theory does not account for the effect of different radial profiles between the incident gust and the duct modes. In what follows we examine, with two test cases, the validity of the strip theory approach regarding these issues and how they affect the aerodynamic and acoustic responses of the blades.

First, we examine the effect of different number of propagating acoustic modes. We consider a rotor/stator interaction problem with a reduced frequency $\tilde{\omega} = 3\pi$, zero upwash radial phase variation $n_g = 0$, and no lean or sweep. The duct has two propagating modes, whereas there is only one propagating mode in the strip theory calculations for $r > 0.737 r_m$. Figure 5 compares the unsteady sectional lift coefficient between the three-dimensional computations and those

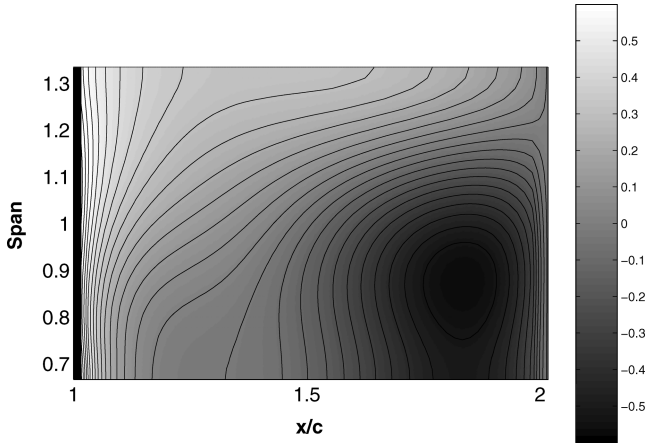

Fig. 6 Real part of the unsteady pressure jump across the vane for zero lean and sweep: $\tilde{\omega} = 3\pi$, $M_x = 0.5$, $r_t/r_h = 2$, $B = 16$, $V = 24$, $n_g = 0$, and $\alpha = \beta = 0$.

calculated by the strip theory. Obviously there are marked differences along the vane span. In the present approach the radiated sound field is directly calculated from the unsteady pressure at the inlet/outlet sections of the computational domain. Figure 6 shows contour plots of the real part of the unsteady pressure difference across the vane for this example. Clearly, the unsteady pressure difference exhibits a complex spanwise pressure distribution, where it is maximum at the leading edge and drops much faster at the hub as we move towards the trailing edge. This case clearly shows that the blade aerodynamic and acoustic responses are quite different from those calculated from the strip theory. Thus, the strip theory is not in general suitable for typical fan noise calculations.

Second, we consider another test case to demonstrate the importance of three-dimensional effects produced by different radial profiles between the incident gust and the duct modes. We also validate our results by comparison with other studies. As in the preceding case, we set the reduced frequency $\tilde{\omega} = 3\pi$, with the same geometry just considered. However, the upwash spanwise phase variation is modified by setting $n_g = 6$. Figure 7 compares spanwise variations of the unsteady pressure jump across the vane at four different chordwise locations, with those calculated by Schulten and Namba.[20] It is clear that the unsteady pressure difference exhibits different behavior along the vane span and that the agreement between the present numerical solution and the benchmark solution is excellent at all axial locations along the blade chord. For $x/c < 0.2$, the unsteady pressure difference has large radial modulation and is strongly correlated to the unsteady gust distribution. For $x/c > 0.2$ the radial modulation of the unsteady pressure difference along the span becomes small, in spite of the upwash large radial phase modulation. This was also found in experiments performed for swept blades at NASA and reported by Envia.[24]

Now, recall that in the strip theory approach the unsteady pressure jump along the vane span will always have the radial phase of the incident disturbance, that is, $\Delta p'(x, r) = \Delta p'(x) \exp[\mathrm{i} n_g (r - r_h)/(r_t - r_h)]$. The numerical results shown in Fig. 7 clearly indicate that this is not the case and that the strip theory approach is not suitable for incident disturbances with large radial phase variations.

Upwash Spanwise Phase Variation

As suggested by Envia and Nallasamy,[10] we presume that the sound power reduction by vane lean and/or sweep is caused by the rotor-wake azimuthal distortion as it interacts with the stator vane, which enhances the upwash phase spanwise variation. Classical single airfoil theory predicts that phase spanwise variations of the incident gust reduces both the unsteady airfoil lift and the scattered sound.[15,25] Moreover, for an annular cascade in a duct Atassi et al.[17] have shown that 1) when the radial phase of the incoming gust is different from that of a given duct mode weak scattering into that

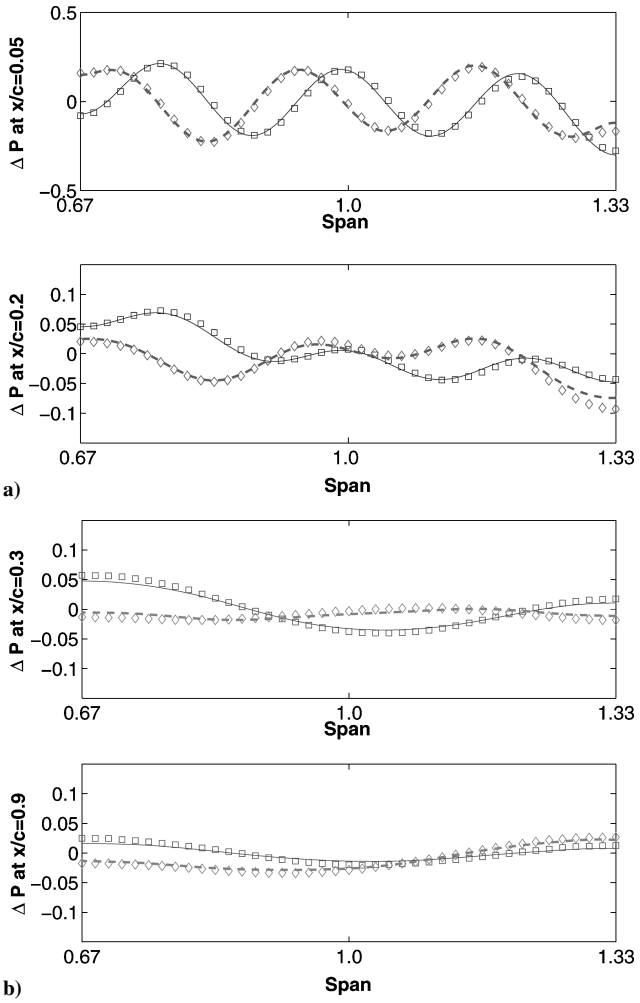

Fig. 7 Spanwise variations of the unsteady pressure jump across the vane compared with those of Schulten at different chordwise locations: Schulten's results are in lines and the present results are in symbols; □ and ——, real part; and ◇ and - - - -, imaginary part of the unsteady pressure. $M_x = 0.5$, $\tilde{\omega} = 3\pi$, $r_t/r_h = 2$, $B = 16$, $V = 24$, $n_g = 6$, and $\alpha = \beta = 0$.

duct mode occurs, and 2) when there are many duct modes with different radial variations from that of the incoming gust the scattered energy is mainly contained in those duct modes with the closest radial variations to the incoming gust. Therefore, we first examine the effects of the upwash spanwise phase variation along the vane span and assess the strength of the coupling between the incident disturbance and the propagating duct modes.

Upstream disturbances (rotor wakes) are nearly convected by the mean flow. These disturbances then interact with the stator vanes. For real fans because of the mean-flow swirl, the rotor wakes are distorted at the leading edge of the stator vanes. To illustrate the effect of the swirling motion on the wakes, we first consider a nonrotating mean flow with an axial rotor-wake defect as shown by the radial white bands in Fig. 8a; the stator leading edges are shown by the dashed line. The wakes convect downstream, and the upwash phase along the span is constant. In Fig. 8b the rotor is rotating, and the mean-flow swirl effect is added; hance, the rotor wakes bend in the azimuthal direction as they reach the stator leading edges and clearly intersect the vanes. This modifies the upwash phase along the stator span. In a similar fashion, the rotor wakes appear distorted with respect to the vanes leading edges with lean and/or sweep. This increases the vanes upwash spanwise phase variations.

An efficient means to study the effects of upwash spanwise variations is to characterize the phase by the parameter n_g in Eq. (7). As mentioned earlier, n_g indicates the number of zero crossings of the disturbance velocity radial profile. Note that n_g is also an in indication of the number of intersections of the wake with the

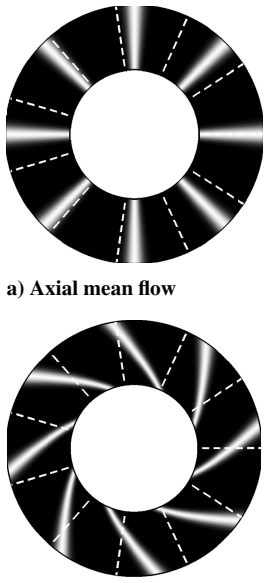

a) Axial mean flow

b) Swirling mean flow

Fig. 8 Intersection of rotor wake (white bands) with stator leading edge (white dashed line) for an axial mean flow and a swirling mean flow.

vane. This is similar to our acoustic modes representation, where the radial modal number n gives the number of zero crossings of the mode radial profile. For $n_g > 0$, the rotor wake at the stator leading edge leads that at the tip as in typical fan designs. Figures 9a and 9b compare the first and second downstream acoustic propagating modes for three test cases with $n_g = 0, 2, 4$. The first mode ($c^{\pm}_{-8,0}$) cuts on at $\tilde{\omega} = 6.2$, and for $6.2 < \tilde{\omega} < 9.2$ it is the only propagating mode. However, as the reduced frequency increases a second mode ($c^{\pm}_{-8,1}$) cuts on. Figure 9a shows that the amplitude of the first acoustic mode ($c^{+}_{-8,0}$) for $n_g = 0$ is much stronger than those for $n_g = 2$ and 4, particularly when there is only one mode propagating. Note that both the incoming disturbance $n_g = 0$ and the scattered first mode $c^{+}_{-8,0}$ have no zero crossings. This also confirms the results of classical single airfoil theory that spanwise phase variations of the incident gust reduces the scattered sound.[25] On the other hand, Fig. 9b shows that when there are two propagating modes the amplitude of the second propagating mode is stronger for the disturbance with a spanwise phase variation $n_g = 2$, followed closely with that for $n_g = 0$. The amplitude of the acoustic mode with $n_g = 4$ remains rather weak. Note that the second acoustic mode $(-8, 1)$ has one radial crossing, whereas the incoming disturbance $n_g = 0$ has no radial crossing and $n_g = 2$ has two radial crossings. This suggests that the scattered acoustic energy of $(-8, 1)$ is strongest for incident disturbances with the closest radial variations to that mode. These results imply that there is significant interaction between the upwash spanwise phase variations and the propagating duct modes. Scattered acoustic modes are more excited by disturbances with similar upwash spanwise phase variations. This is similar to conclusions found by Atassi et al.,[17] where the upwash spanwise amplitude was varied and the correlation between these disturbances and the radiated sound pressure was examined. Their results show that the amplitude of the scattered sound modes was stronger when they have similar variations in the radial direction as that of the incident disturbance.

Figure 10 compares the amplitude of the unsteady sectional lift coefficient $|c_{l'}|$ at the mean radius for $n_g = 0, 2, 4$. For $n_g = 0$ and at the lower frequency range, $|c_{l'}|$ is initially much larger than for $n_g = 2$ and 4 but drops significantly as the frequency approaches 6.2 at which the first modes cuts on. For $n_g = 2$, $|c_{l'}|$ begins to rise as the frequency increases until it reaches the second cut-on frequency 9.2. Although both the aerodynamic and acoustic responses strongly depend on the duct modes, the variation of $|c_{l'}|$ is not the same as that of the $|c^{\pm}_{\mathrm{mn}}|$.

We now examine the correlation between the radial variation of the upstream disturbance with that of the sectional lift coefficient

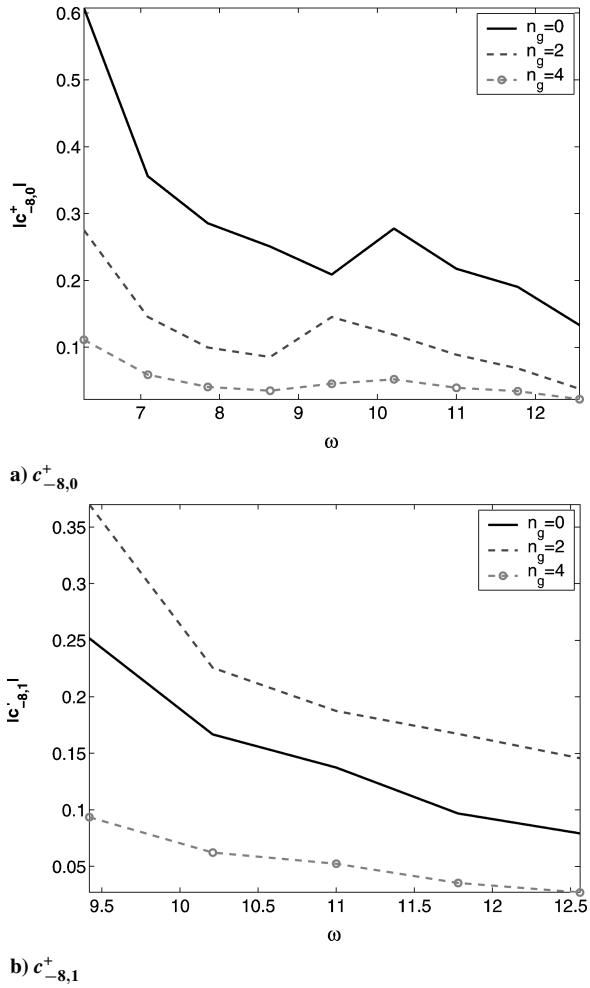

Fig. 9 Amplitude of the downstream pressure coefficient $|c^+_{mn}|$ vs the reduced frequency $\tilde{\omega}$ for $n_g = 0, 2, 4$; $M_x = 0.5$; $r_t/r_h = 2$; $B = 16$; and $V = 24$.

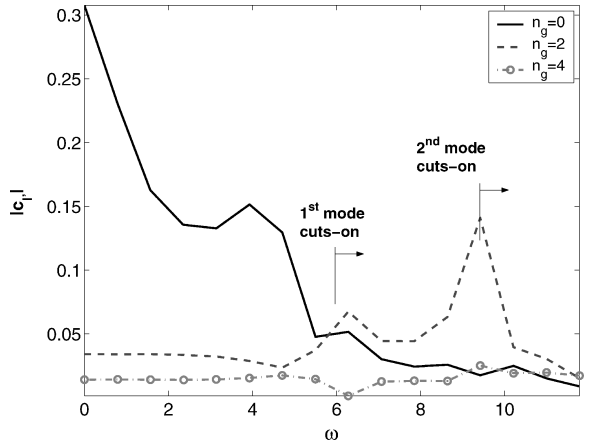

Fig. 10 Amplitude of the unsteady sectional lift coefficient at the mean radius vs the reduced frequency $\tilde{\omega}$ for $n_g = 0, 2, 4$; $M_x = 0.5$; $r_t/r_h = 2$; $B = 16$; and $V = 24$.

along the span. Figure 11 shows the span variation of $|c_{l'}|$ for $n_g = 2$ at two different frequencies. For $\tilde{\omega} = \pi$, where no modes are cut on, the lift distribution along the span is uncorrelated to the blade upwash spanwise variation. For $\tilde{\omega} = 4\pi$, with four acoustic modes cut on, there is more radial variation suggesting some coupling between the upwash radial variation and the unsteady sectional lift. This further demonstrates that the strip theory approximation can lead to erroneous results because the radial variation in unsteady pressure and sectional lift cannot in general be factored out.

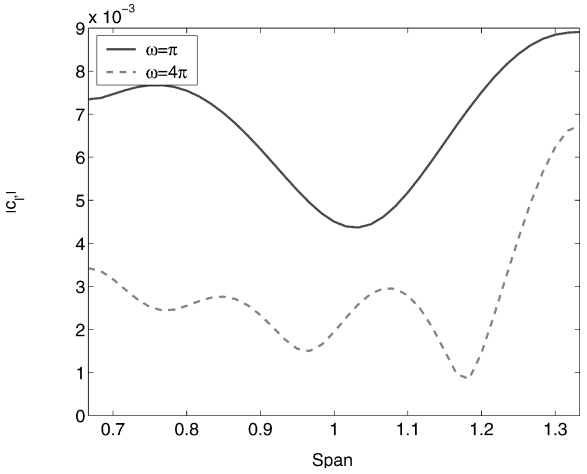

Fig. 11 Amplitude of the unsteady sectional lift coefficient along the blade span for $n_g = 2$, $M_x = 0.5$, $r_t/r_h = 2$, $B = 16$, $V = 24$, and $\tilde{\omega} = \pi, 4\pi$.

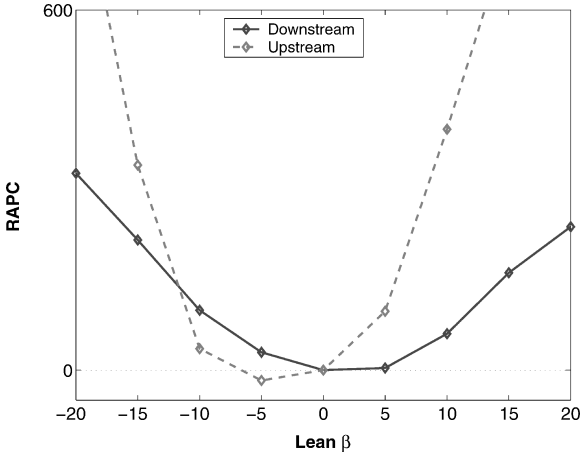

a) Case 1: $B = 23$, $V = 24$

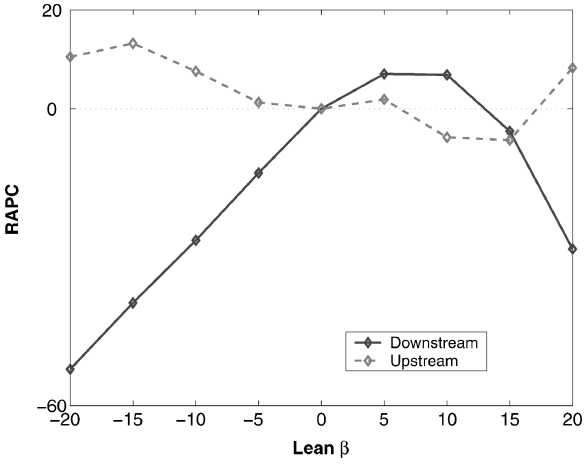

b) Case 2: $B = 16$, $V = 24$

Fig. 12 RAPC for downstream and upstream sound power levels for different lean angles for both test geometries: ——, downstream and - - - -, upstream sound power change. $\tilde{\omega} = 3\pi$, $M_x = 0.5$, and $r_t/r_h = 2$.

Noise Control by Vane Lean

Lean is defined as the azimuthal displacement β of the vane leading edge from its baseline radial position, as shown in Fig. 2. The lean angle is defined as positive in the counterclockwise direction. With this definition, positive lean corresponds to the azimuthal direction of propagation of the upstream disturbances considered in the present work. Spanwise phase variation of the disturbance upwash will depend on the lean angle. This phase variation is responsible for

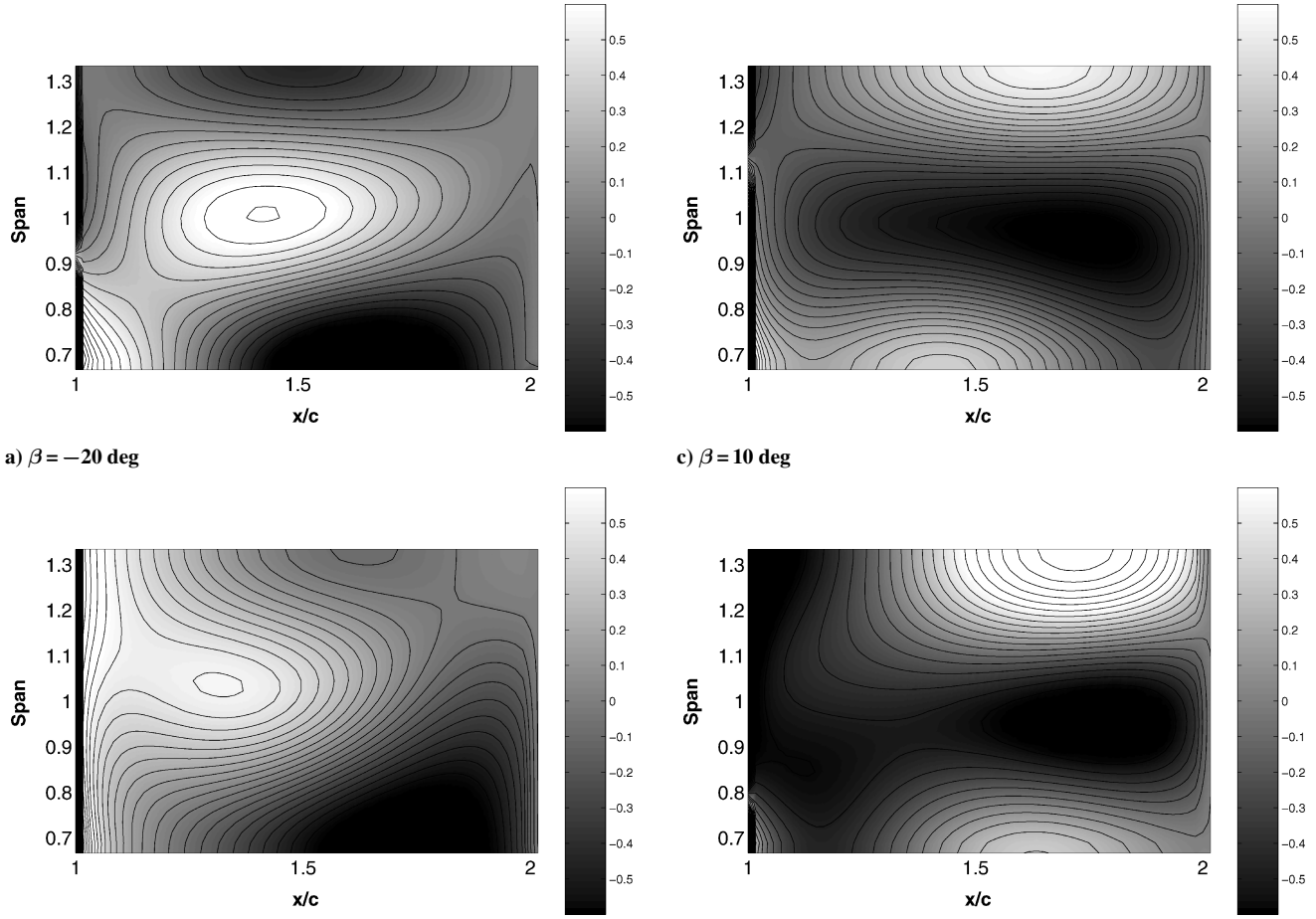

a) $\beta = -20$ **deg** **c)** $\beta = 10$ **deg**

b) $\beta = -10$ **deg** **d)** $\beta = 20$ **deg**

Fig. 13 Real part of the unsteady pressure jump across the vane for different lean angles: $\tilde{\omega} = 3\pi$, $M_x = 0.5$, $r_t/r_h = 2$, $B = 16$, and $V = 24$.

the noise reduction or amplification. Thus we can argue that increasing vane lean, which increases the incident disturbance spanwise phase variation, will also reduce the perceived noise levels. However, this might not be always the case. Schulten,[12] has reported results that show that vane lean increases the noise level and the quietest configuration is for zero vane lean. On the other hand, Envia and Nallasamy[10] have concluded that lean is usually effective in the negative direction. In this section we examine the results found in the previous studies and attempt to resolve the differing conclusions.

We consider two test geometries with $r_t/r_h = 2$ and $M_x = 0.5$ for the same incident disturbance with a reduced frequency $\tilde{\omega} = 3\pi$ and $n_g = 0$. For the first geometry, $B = 23$, $V = 24$, $p = 1$, and hence $m_g = 23$. There are three propagating duct modes ($c_{-1,0}$, $c_{-1,1}$, $c_{-1,2}$). This case is similar to that studied by Schulten.[12] For the second geometry, $B = 16$, $V = 24$, $p = 1$, and $m_g = 16$. This is a more relevant case for a real engine configuration. For that case there are two propagating duct modes ($c_{-8,0}$, $c_{-8,1}$). These test cases are carried out to 1) compare and validate our results with those of Schulten and 2) examine the effectiveness of vane lean for realistic fans.

Validation Case: $B = 23$, $V = 24$

For this test case the number of rotor blades and stator vanes are chosen so that the propagating modes have an azimuthal mode number $m = -1$. Figure 12a shows the RAPC vs the lean angle. It is clear that lean is totally ineffective for this rotor/stator configuration with a significant power increase for any lean angle. These results are in agreement with calculations performed by Schulten for a similar geometry.

Benchmark Case: $B = 16$, $V = 24$

For the benchmark test case the number of rotor blades and stator vanes are chosen so that the propagating duct modes have an azimuthal mode number $m = -8$. Figure 12b shows the RAPC vs the lean angle. The downstream sound power is significantly reduced for negative and for large positive lean angles. However, lean is not effective for the upstream sound power.

To show that the vane lean introduces spanwise pressure variations, the real part of the unsteady pressure difference along the vane span for four lean angles is shown Fig. 13. The first two plots (a and b) are for negative lean, $\beta = -20$ and -10 deg, respectively, and plots c and d are for positive lean, $\beta = 10$ and 20 deg, respectively. There is significant spanwise pressure variation associated with vane lean compared to the case of zero lean shown in Fig. 6.

Analysis of Lean Effectiveness

Figure 12 shows that vane lean can be effective or ineffective depending on the rotor/stator geometry. This seems to counter the classical results mentioned earlier that an oblique gust reduces the unsteady lift and scattered sound power.[15,25] However, here we are dealing with the acoustic modes in a duct, and as we have mentioned earlier the cascade aerodynamic and acoustic responses strongly depend on the composition of the duct modes. To understand and explain the results of Fig. 12, we examine the modal composition of the propagating modes.

Lean generates a spanwise phase variation of the disturbance upwash on the vane surface. For a uniform flow this phase variation is proportional to $(m_g \beta)$. Thus the larger the lean angle β, the stronger the phase variation. As shown in the first section of the results, radial gust variations excite and couple with higher-order propagating modes. Because of the spanwise phase variation caused by vane lean, the amplitude of the first propagating mode is reduced, whereas the amplitude of the higher-order modes can increase. As a result, for lean to be effective the acoustic power contributed by the first propagating mode must decrease at a faster rate than that at which the acoustic power contributed by the higher-order modes. Because

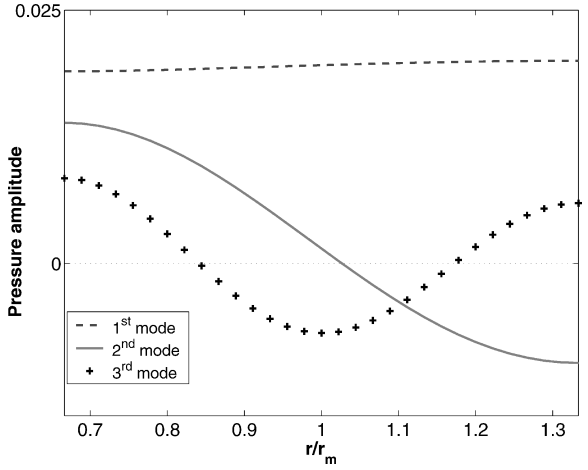

a) Case 1: $B = 23$, $V = 24$

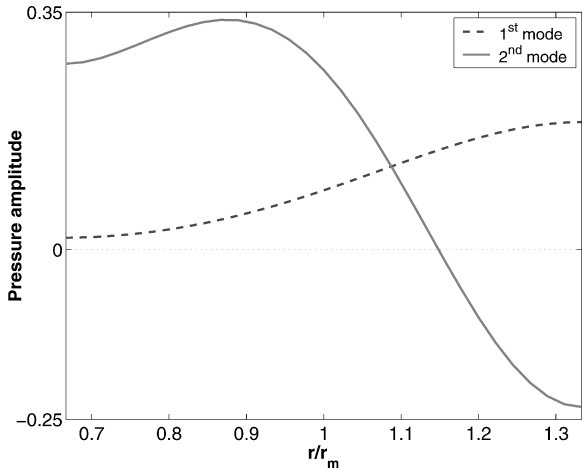

b) Case 2: $B = 16$, $V = 24$

Fig. 14 Spanwise variation of the real part of the unsteady pressure of the acoustic propagating modes for the two test cases at zero lean: $\tilde{\omega} = 3\pi$, $M_x = 0.5$, and $r_t/r_h = 2$.

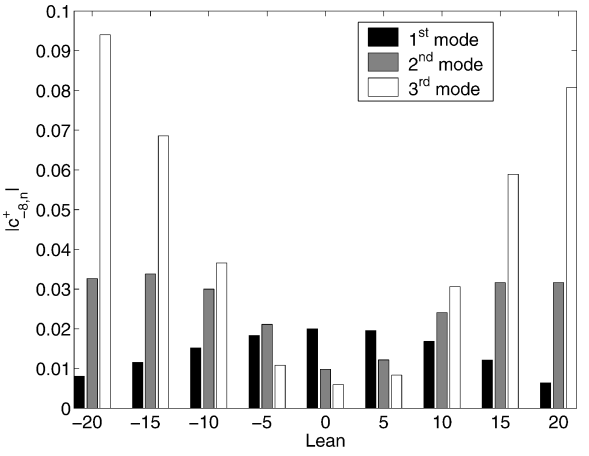

a) Case 1: $B = 23$, $V = 24$

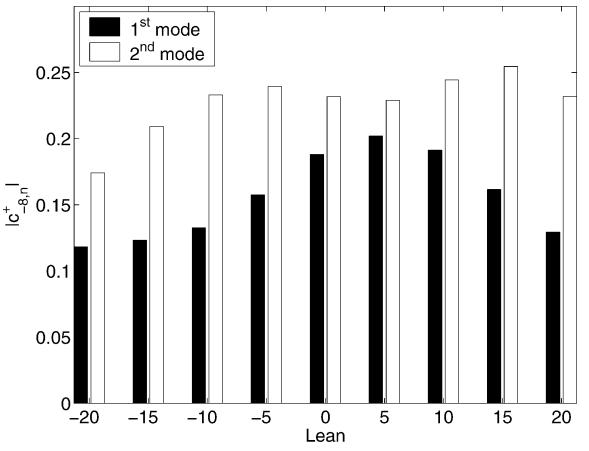

b) Case 2: $B = 16$, $V = 24$

Fig. 15 Comparison of downstream acoustic pressure amplitudes for different lean angles: $\tilde{\omega} = 3\pi$, $M_x = 0.5$, and $r_t/r_h = 2$.

the number and the radial profile of the propagating modes $\mathcal{P}_{\mathrm{mn}}(r)$ are independent of the lean angle and only their amplitude c_{mn} varies with lean, we examine the variation of the acoustic coefficients c_{mn} for different lean angles for the two test cases. We first show in Fig. 14 the spanwise variation of the real part of the acoustic pressure $\Re(c_{\mathrm{mn}}\mathcal{P}_{\mathrm{mn}})$ for both test geometries with zero lean. Figure 15 compares the amplitudes of the downstream acoustic modes $|c_{\mathrm{mn}}|$ for various lean angles for both test geometries.

For the first test case, the first propagating mode is almost a plane wave, and the amplitude of the downstream acoustic pressure coefficient decreases as lean is varied from zero to ± 20 deg as seen in Fig. 15a. However, the second and third modes amplify at a faster rate than that at which the first mode is reduced. This accounts for the relative power increase with various lean angles and explains the conclusions of Schulten that lean is ineffective. However, we note that Schulten's conclusions are not general as we have just shown, and that he found reductions for lean with one propagating mode cut on.

Schulten suggested that the azimuthal mode number m of the propagating modes is not likely responsible for the increase in the sound power as shown in Fig. 12. Rather he attributed this rise to the radial force component acting on the vanes as a result of the lean. We note that Schulten built his conclusions on a single case where $m = -1$. Our results for $m = -8$ show a significant reduction in the acoustic power, thus indicating the importance of the modal composition and the coupling of the cascade response with the gust radial variations.

We now consider the second test case. For negative lean angle β, the amplitude of the first acoustic mode decreases as β decreases from 0 to -20 deg, whereas the amplitude of the second acoustic mode first increases and then decreases, as shown in Fig. 15b. The increase in the amplitude of the second mode, however, is smaller than the decrease of that of the first mode, thus resulting in reduction of the overall sound power. Similarly, as the amplitude of the first mode decreases for large positive lean angles, the positive lean becomes efficient in the overall sound power reduction, as shown in Fig. 12b.

Envia and Nallasamy[10] suggested that the application of lean and/or sweep is effective if the number of rotor-wake intersections with the stator leading edge is increased. This is partly true; however, it is should not be taken as a design rule. From Figs. 6 ($\beta = 0$) and 13c ($\beta = 10$ deg), we find that the rotor wake does intersect with the stator vane for $\beta = 10$ deg; however, for this case the radiated sound power is amplified. This is because of the contribution to the sound power from the second propagating duct mode, which has amplified. Thus the design rule of Envia and Nallasamy is not valid for all cases. We propose the following new rule: Lean is always effective if the number of rotor-wake intersections with the stator vanes is larger than the number of propagating duct modes.

Lean can be tailored to reduce the intensity of a given duct mode. For example, as seen in the preceding section, if the spanwise upwash phase variation is large, $n_g = 4$, and there are two propagating duct modes, the amplitude of the second mode will be small compared to the case of $n_g = 2$ (as seen in Fig. 9b). If vane lean was designed such that the number of rotor-wake intersections with the stator vane is 4, lean would be extremely effective because the amplitude of first and second propagating duct modes will be reduced.

Lean Effectiveness at Different Reduced Frequencies

The reduced frequency affects the number of propagating modes in the duct. As a result, lean effectiveness strongly depends on the

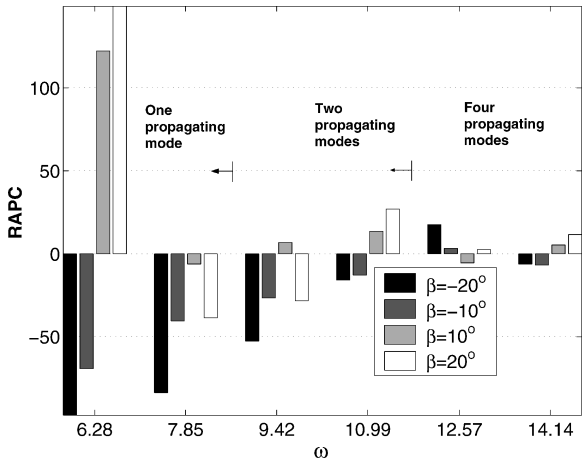

Fig. 16 Comparison of downstream RAPC for different stator lean angles vs the reduced frequencies in a uniform flow: $M_x = 0.5$, $r_t/r_h = 2$, $B = 16$, and $V = 24$.

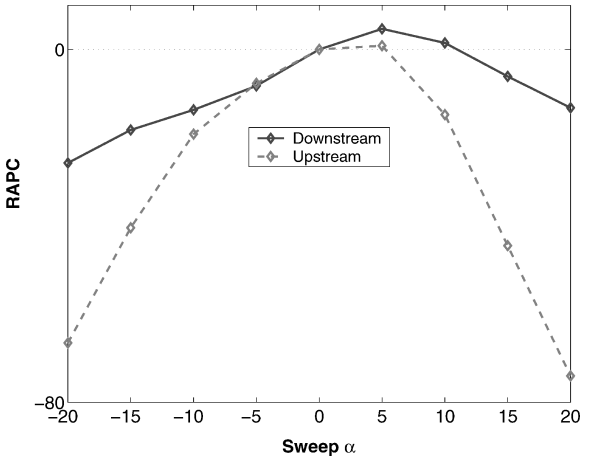

Fig. 17 RAPC for downstream and upstream power levels for different sweep angles: $M_x = 0.5$, $r_t/r_h = 2$, $\tilde{\omega} = 3\pi$, $B = 16$, and $V = 24$.

reduced frequency. Figure 16 compares the downstream RAPC for different lean angles at different reduced frequencies. For the first two frequencies $\tilde{\omega} = 2\pi, 2.5\pi$ there is one propagating mode; thus, the sound power is significantly reduced for negative lean. For the third and fourth cases there are two propagating modes, and the effectiveness of lean is reduced. This is because of the relative increase in amplitude of the second mode over that of the first mode. For the last two test frequencies $\tilde{\omega} = 4\pi, 4.5\pi$, there are four propagating modes ($c_{-8,0}$, $c_{-8,1}$, $c_{-8,2}$, $c_{16,0}$), and lean becomes even less effective. For $\tilde{\omega} = 4\pi$, except for $\beta = 10$ deg, the drop in the amplitude of the first mode no longer overcomes the increase in amplitude of the higher-order modes.

Noise Control by Vane Sweep

Sweep as lean is another noise-reduction mechanism. Backward sweep is defined as the axial displacement of the vane leading edge from its baseline radial position, as shown in Fig. 2. Vane sweep modifies the spanwise phase variation of the incident gust as does lean. For the case of a uniform flow, the disturbance upwash phase variation is proportional to $[(\omega/U_x)\Delta r \tan\alpha]$. Increasing the sweep angle and/or the reduced frequency will increase the rotor-wake intersections with the vane leading edge.

As for the case of lean, numerical calculations are validated by comparison with the results of Schulten[13] and Envia and Nallasamy.[10] Schulten has concluded that for high Mach number sweep is only effective for large backward sweep angles and that for small backward sweep angles sweep is ineffective and there might be an increase in the noise level. His results also suggest that noise reduction by vane sweep depends on the azimuthal mode number of the propagating duct modes. Furthermore, he has shown that sweep is more effective for reducing upstream noise levels than downstream noise levels. Envia and Nallasamy have presented experimental evidence demonstrating sweep effectiveness for large backward sweep angles and numerical results, which suggested that backward sweep is always effective and forward sweep is always ineffective. In what follows we attempt to resolve these differing conclusions.

Benchmark Case: $B = 16$, $V = 24$

Figure 17 compares the upstream and downstream RAPC vs the sweep angle α. Here $M_x = 0.5$, $n_g = 0$, $\tilde{\omega} = 3\pi$, and $r_t/r_h = 2$. The upstream acoustic power level is reduced for both backward and forward sweep. On the other hand, there is a reduction in the downstream sound power for forward sweep and an initial increase for small backward sweep angles, confirming the results calculated by Schulten.[13] The downstream sound power decreases for sweep angles larger than 12.5 deg. We define the angle of effective sweep as the smallest angle at which the downstream sound power decreases. Note that the rate of sound power reduction is larger for sound propagating upstream than downstream. The stronger reduction can be caused by the difference in the axial wavelength for the propagating duct modes. Because of the fluid motion, the upstream axial wavelength is smaller than the downstream wavelength. These results are in good agreement with those of Schulten for the same geometry and Mach number. In fact, Schulten predicts the angle of effective sweep to be about 12 deg and that the reduction rate in the upstream sound power is much larger than the downstream sound power.

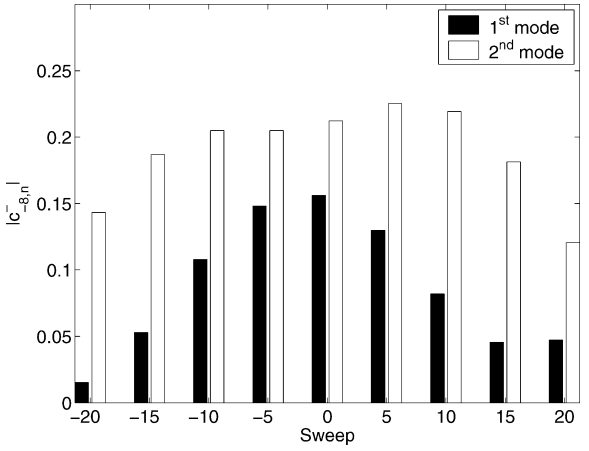

a) Upstream

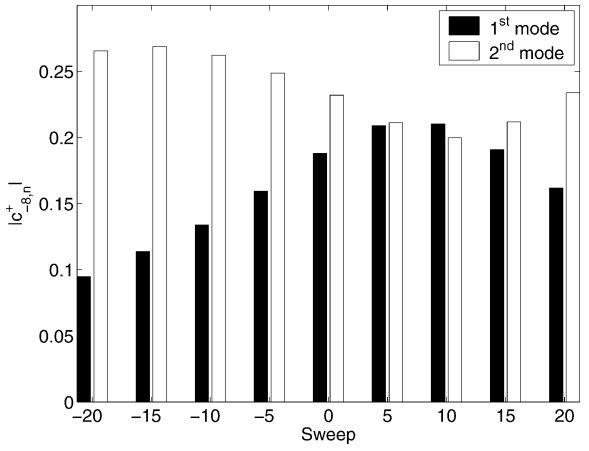

b) Downstream

Fig. 18 Comparison of the amplitude of the acoustic pressure coefficients for different sweep angles: $\tilde{\omega} = 3\pi$, $M_x = 0.5$, $r_t/r_h = 2$, $B = 16$, and $V = 24$.

Figure 18 compares the amplitudes of the upstream and downstream acoustic modes $|c^{\pm}_{mn}|$ for various sweep angles. The first

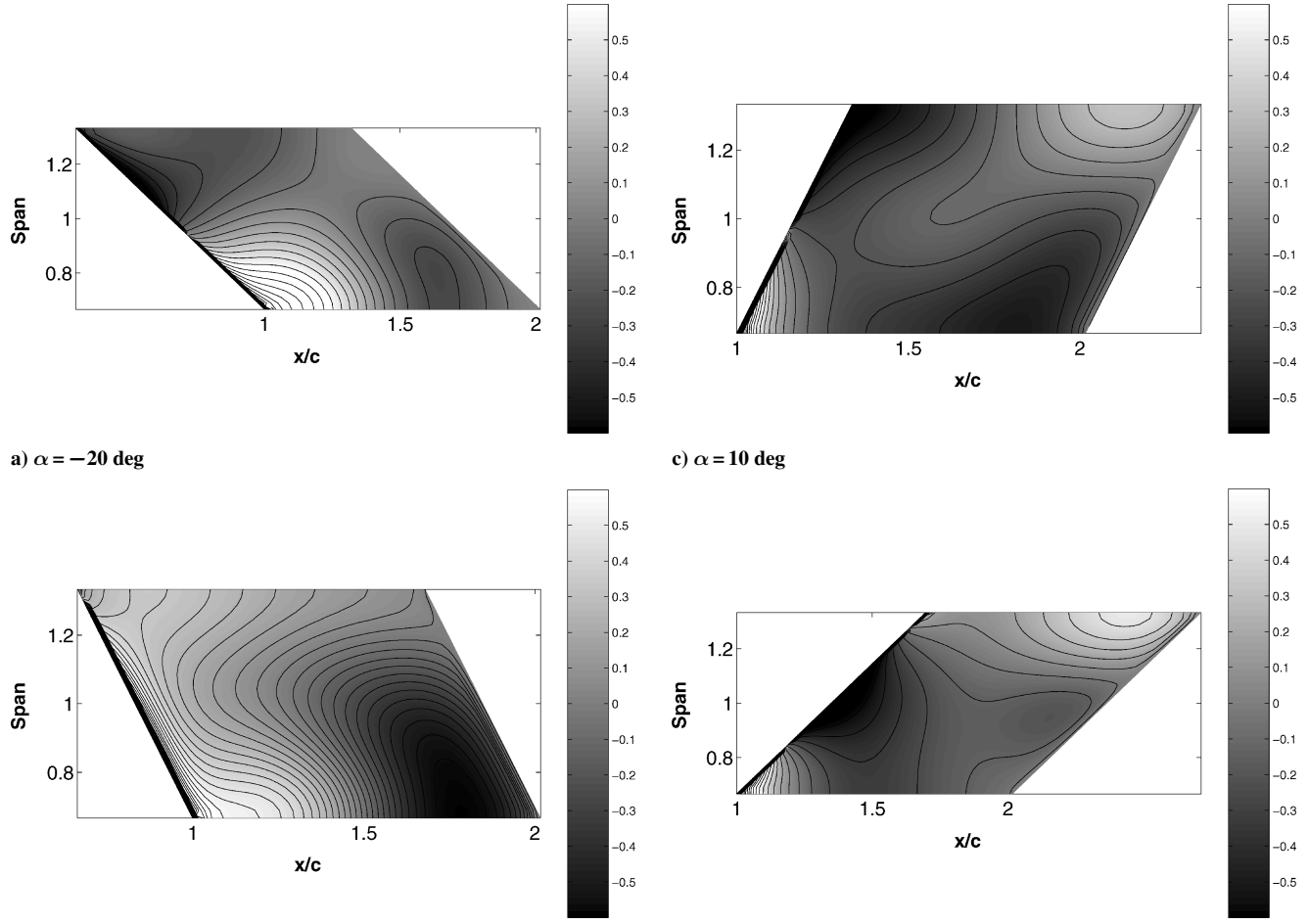

Fig. 19 Real part of the unsteady pressure jump across the vane for different sweep angles $\tilde{\omega} = 3\pi$, $M_x = 0.5$, $r_t/r_h = 2$, $B = 16$, and $V = 24$.

propagating mode upstream is significantly reduced by vane sweep, which results in the overall reduction of the upstream power content. The first mode downstream, however, increases for backward sweep for angles up to 10 deg and then decreases, thus reducing the overall propagating sound power.

Our numerical results indicate that forward sweep is effective. Envia and Nallasamy[10] used a strip theory approach, which suggested that sweep was only effective for backward sweep. The differences between the present results and theirs are attributed to two factors:

1) In their model, the viscous wake decay was accounted for and thus the upwash of the wake is different for backward and forward sweep. In our model we do not account for wake decay; however, we believe it is unlikely to introduce such significant changes.

2) Our computations are three-dimensional, which are different at high frequency from the strip theory approach used in their model.

As for the case of vane lean, we show that the vane sweep introduces spanwise phase variations along the span. The real part of the unsteady pressure difference along the vane span for four cases is shown in Fig. 19. The first two plots (a and b) are for forward sweep, $\alpha = -20$ and -10 deg, respectively, and plots c and d are for backward sweep, $\alpha = 10$ and 20 deg, respectively. As with vane lean, there is a significant spanwise variation in the real part of the unsteady pressure jump across the vanes associated with vane sweep compared to the case of zero lean and sweep shown in Fig. 6.

Sweep Effectiveness at Different Reduced Frequencies

Similar to lean, sweep is not effective for incoming gusts at all reduced frequencies because it depends on the number of propagating modes. Figure 20 compares the downstream RAPC for different sweep angles at different reduced frequencies. Earlier it was mentioned that for a reduced frequency $\tilde{\omega} = 3\pi$ the effective sweep

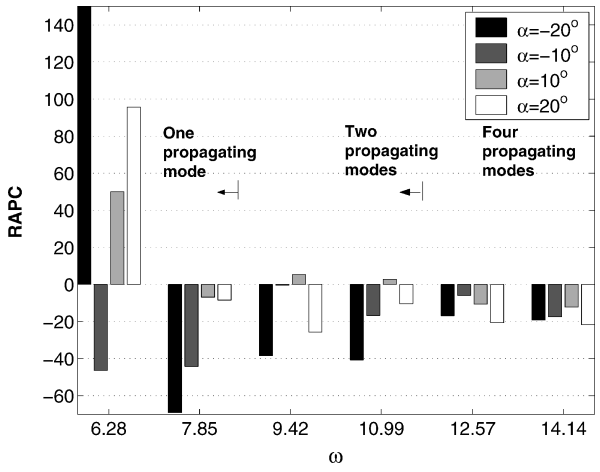

Fig. 20 Comparison of the downstream RAPC for different stator sweep angles vs reduced frequencies in a uniform flow with $M_x = 0.5$, $r_t/r_h = 2$, $B = 16$, and $V = 24$.

angle is approximately 12.5 deg. Comparing the power reduction at $\tilde{\omega} = 3\pi, 3.5\pi, 4\pi$ suggests that this angle decreases as the frequency increases. Note that for $\tilde{\omega} = 2\pi$, forward sweep is ineffective.

Vane Lean or Sweep: The Design Rule

The efficiency of vane lean or sweep for tonal noise reduction depends on the similarity or difference between the radial profiles of the propagating modes and the incident gust. In our present model, this is quantified with the radial mode numbers n_g and n for the incident gust and the cut-on acoustic modes, respectively. As we

apply lean and/or sweep, we modify n_g, and, as a result, the amplitude of some propagating duct modes will increase while others will decrease. The contribution of these modified modes to the overall sound power is what will determine the design efficiency in reducing the radiated sound. The number and radial profile of the acoustic propagating modes will indicate the optimum shape for the rotor wakes as they intersect the vane leading edge and determine the vane upwash.

Therefore to optimally design a stator vane with lean and/or sweep, we must first calculate the number of propagating duct modes. These are calculated from the design operating conditions and the number of rotor blades and stator vanes. Then we can choose suitable lean and/or sweep angles for optimal rotor-wake intersections with the vane leading edge. The number of intersections (zero crossings of the upwash radial profile) must be larger than the number of propagating modes. If this is not achievable, lean and sweep can be tailored to reduce the amplitude of the lower-order acoustic modes. Passive liners can then be used to effectively attenuate the higher-order acoustic modes.[26] As a rule of thumb, negative lean is more beneficial than positive lean angles, and large backward sweep is essential. However, it is advisable to validate these results numerically at the design stage.

The results in Figs. 16 and 20 suggest that the noise-reduction mechanism for vane sweep is more effective than that for vane lean for a broad range of frequencies, that is, different operating conditions. These results also suggest that vane lean will be ineffective for broadband noise reduction, where the number of propagating modes is large corresponding to a continuous spectrum for all azimuthal mode numbers m. For large $|m|$, the number of propagating modes is small, and lean will be effective; however, for small $|m|$ there is a large number of propagating modes, and lean is ineffective. Thus for a broad range of frequencies, we can expect more attenuation for large $|m|$, that is, for small disturbance scales.

Noise Control by Mean-Flow Acceleration

Most turbofan engines have nonuniform ducts. The inlets have larger tip-hub ratios compared to those at outlets. This results in a different number of propagating modes at outflow and inflow. In extreme cases of low frequency, the inflow section might have propagating modes, and the outflow might have none. When this occurs, sound will only radiate upstream. A study is performed to examine the effectiveness of converging annular ducts for sound power reduction.

We consider two different test cases in this paper. In the first case we consider a variable mass flow rate at inflow, such that the exit Mach number is constant. Holding the exit Mach number constant is important for component noise design because jet noise (not considered here) could become significant as the exit Mach number increases. In the second case we fix the mass flow rate at inflow and have a variable exit Mach number.

The mean flow used in these computations is the solution of the full nonlinear steady Euler equations. As shown in the formulation section, the unsteady flow is linearized about this nonlinear mean flow. The numerical scheme was first validated by testing the propagation of an incident acoustic wave in a variable converging-diverging duct. Excellent agreement was found between the computed results and those of a high-frequency multiple scales solution by Rienstra[27] and are presented by Elhadidi.[8]

We consider the case with a disturbance reduced frequency $\tilde{\omega} = 3\pi$ and $n_g = 0$. The normalization is based on the mean radius and the speed of sound at inflow. For both test cases, $B = 16$, and $V = 24$. At the inlet section, the tip radius $r_t = \frac{4}{3}$, and the hub radius $r_h = \frac{2}{3}$. The tip radius is fixed throughout the analysis. The chord $c = 2\pi r_m / V$ and the computational domain $L = 3c$. The hub radius is defined by

$$
\begin{aligned}
x \le c &\Rightarrow r = r_1 \\
c < x < 2c &\Rightarrow r = r_1 + 3(r_2 - r_1)(x/c - 1)^2 \\
&\quad -2(r_2 - r_1)(x/c - 1)^3 \\
x \ge 2c &\Rightarrow r = r_2
\end{aligned}
$$

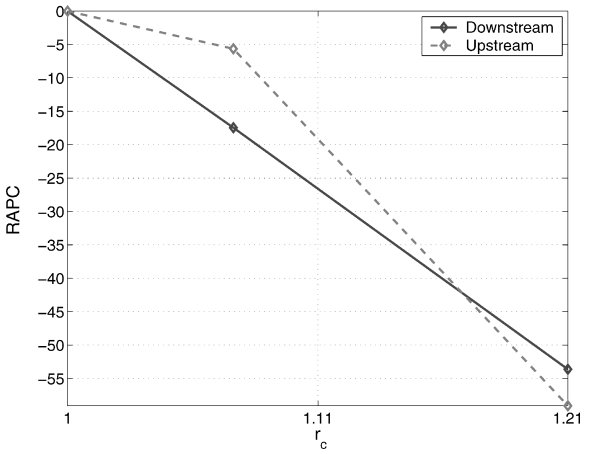

a) Fixed exit Mach number

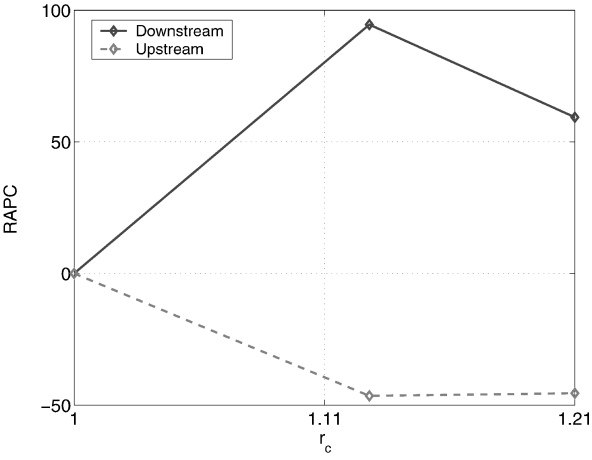

b) Fixed inlet Mach number

Fig. 21 RAPC for the downstream and upstream sound power levels as a function of the convergence ratio.

Here r_1, r_2 are the hub radii at inlet and exit, respectively. We define the duct convergence ratio $r_c = r_2/r_1$. For this converging annular duct, $\mathrm{d}r/\mathrm{d}x = 0$ for $x = c, 2c$, thus ensuring that the mean flow at inflow and outflow are axial and uniform.

Fixed Exit Mach Number

We consider three different annular duct geometries with 1) $M_{x(\text{in})} = M_{x(\text{out})} = 0.5$, $r_c = 1$; 2) $M_{x(\text{in})} = 0.45$, $M_{x(\text{out})} = 0.5$, $r_c = 1.07$; and 3) $M_{x(\text{in})} = 0.4$, $M_{x(\text{out})} = 0.5$, $r_c = 1.21$. These geometries have been chosen to satisfy the conservation of mass under isentropic conditions. For the three geometries considered, there are two propagating downstream modes ($c^+_{-8,0}$, $c^+_{-8,1}$). At inflow, there are two propagating modes ($c^-_{-8,0}$, $c^-_{-8,1}$) for the first two cases and one propagating mode ($c^-_{-8,0}$) for the last case. Figure 21a shows the RAPC for various duct convergence ratios. The RAPC is calculated using the reference sound power of case 1. The results indicate that there is a significant reduction for both upstream and downstream sound power levels. The reduction of the downstream acoustic power is attributed to the reduction of the amplitude of the propagating modes as seen in Fig. 22a. Similarly, the upstream sound power is reduced because the amplitude of the first mode decreases as we increase the convergence ratio. For the test geometry 3, the reduction of the radiated sound power is even more pronounced because there is only one upstream propagating mode.

Constant Inflow Mach Number

Similar to the previous study, we consider three different annular duct geometries with 1) $M_{x(\text{in})} = M_{x(\text{out})} = 0.4$, $r_c = 1$; 2) $M_{x(\text{in})} = 0.4$, $M_{x(\text{out})} = 0.45$, $r_c = 1.12$; and 3) $M_{x(\text{in})} = 0.4$, $M_{x(\text{out})} = 0.5$,

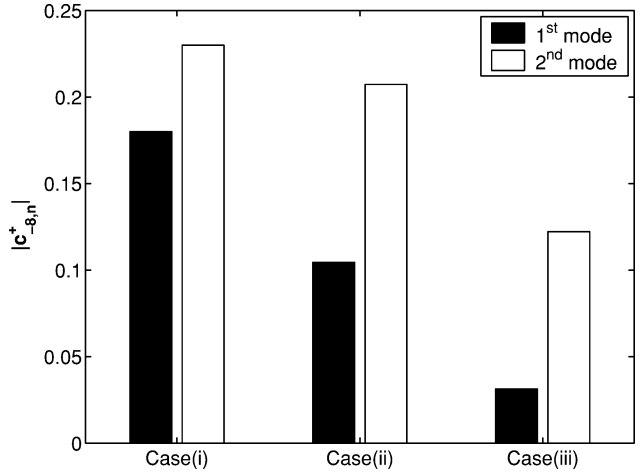

a) Fixed exit Mach number

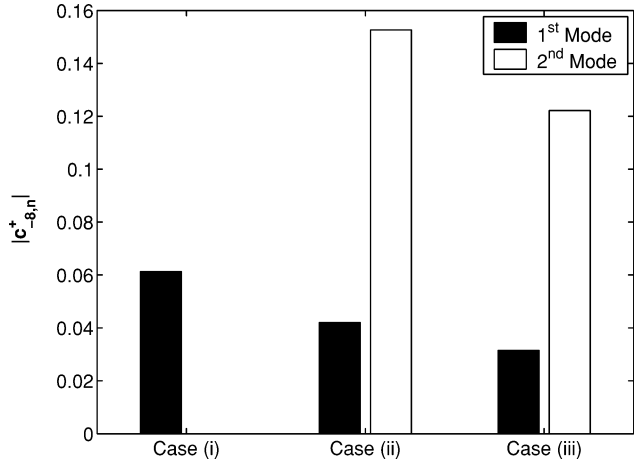

b) Fixed inlet Mach number

Fig. 22 Comparison of the downstream acoustic pressure amplitude as a function of the convergence ratio.

$r_1 = 1.21$. In this case there is one upstream propagating mode ($c^-_{-8,0}$) for all cases. At outflow there is one propagating downstream mode ($c^+_{-8,0}$) for the first case and two propagating downstream modes ($c^+_{-8,0}$, $c^+_{-8,1}$) for the last two cases. The RAPC is calculated with using the reference sound power of case 1. Figure 21b shows the RAPC for the different duct convergence cases, and the results show a significant reduction for the scattered upstream sound power, whereas there is significant increase in the scattered downstream sound power. The upstream sound power is reduced because the amplitude of the upstream mode reduces as we increase the convergence ratio. The downstream behavior can be easily explained in view of Fig. 22b. The first mode decreases as the convergence ratio increases; however, as the second mode cuts on the propagating sound power increases. As we further increase the convergence ratio, while maintaining two propagating downstream modes, the sound power is reduced because the second mode begins to attenuate.

Analysis of Results: The Design Rule

Figure 23 shows the real part of the unsteady pressure jump along the vane span for three of the test cases. Clearly, increasing the duct convergence ratio increases the pressure variations along the vane surface, which is caused by the nonuniformity of the mean flow. This results in a reduction of propagating duct modes amplitude as seen from Fig. 22. Here the upwash is not modified by vane lean and sweep; however, it is modified by the mean-flow nonuniformity. The results suggest that this is also a strong sound-reduction mechanism.

To benefit from converging annular ducts, we must avoid higher-order modes cutting on. This can be achieved by examining the

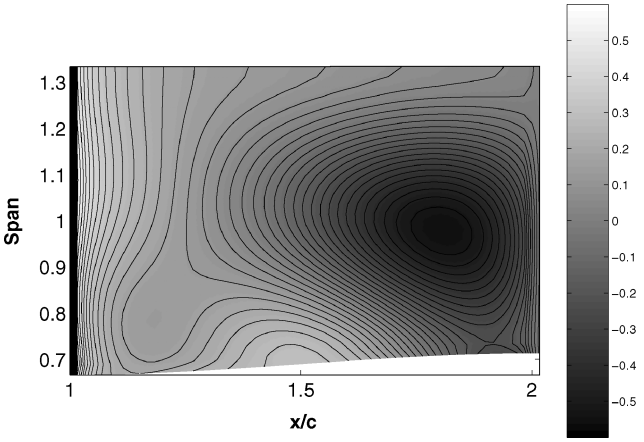

a) $M_{x(\text{in})} = 0.45$, $M_{x(\text{out})} = 0.5$, $r_c = 1.07$

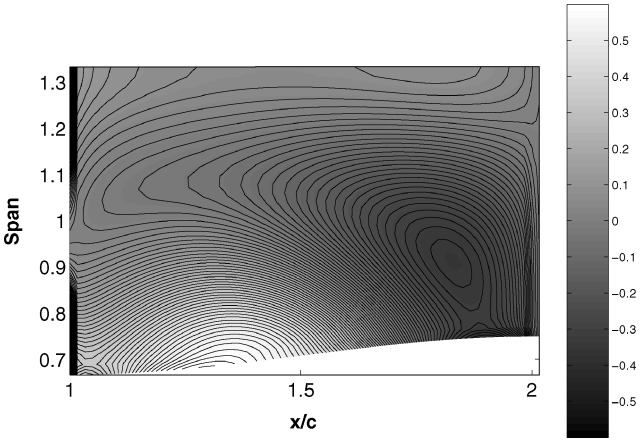

b) $M_{x(\text{in})} = 0.4$, $M_{x(\text{out})} = 0.45$, $r_c = 1.12$

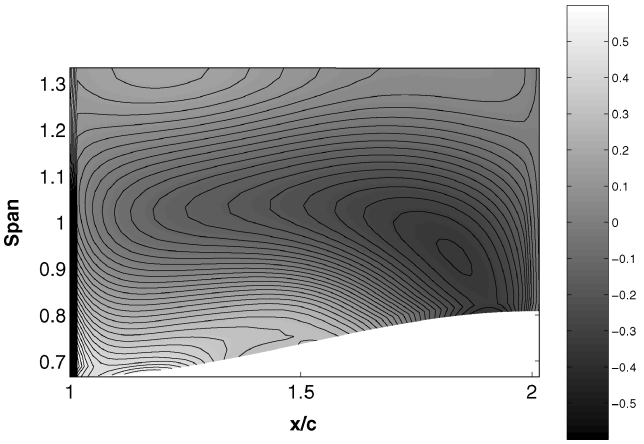

c) $M_{x(\text{in})} = 0.4$, $M_{x(\text{out})} = 0.5$, $r_c = 1.21$

Fig. 23 Real part of the unsteady pressure jump across the vane for different lean angles: $\tilde{\omega} = 3\pi$, $B = 16$, and $V = 24$.

number of cut-on modes for each outflow condition. For example, if there are two outgoing modes we can increase the duct convergence ratio until the third mode is about to cut on. This will ensure good sound reduction.

Conclusions

A three-dimensional Euler model has been developed for fan noise associated with rotor wakes' interaction with stator vanes. The stator is represented by an isolated annular cascade of unloaded blades subject to imposed upstream disturbances. The effects of vane lean and sweep on the aerodynamic and acoustic response of an annular cascade have been analyzed. The results are first compared with those of the strip theory and show that three-dimensional

models are essential and must be considered because of the strong dependence of the cascade acoustic response on the interaction between the acoustic duct modes and the incident disturbances radial profiles.

The main mechanism through which lean and sweep affect the annular cascade response is by modifying the radial variation of the incoming gust. Thus, we have examined the effect of radial phase change on unswept and unleaned vanes. The results showed that variations in the radial phase excite higher-order modes and suggested a modal analysis to analyze the cases of vane lean and sweep.

Results for lean and sweep show that they enhance the rotor-wake radial variations at the stator leading edge, thus increasing the upwash spanwise phase variation. In turn, this modifies the amplitude of the propagating duct modes. For vane lean or sweep to be effective, the contribution of the radiated sound power of all of the propagating duct modes must result in an overall sound power reduction. This can be achieved if the number of rotor wakes' radial profile zero crossings (intersections with the stator vanes) is larger than the number of propagating duct modes. This will ensure that the higher-order cut-on duct modes are not dominant and highly energized.

The effectiveness of vane lean or sweep depends on the number of propagating duct modes; thus, it will depend on the reduced frequency and azimuthal mode number of the propagating duct modes. The results indicate that vane lean effectiveness reduces as the number of propagating modes increase. Thus for low values of the azimuthal mode numbers $|m|$, lean will be only effective for very low reduced frequencies. For higher reduced frequencies vane lean will mainly affect the smaller scales (large azimuthal mode numbers m). Numerical results suggest than vane sweep is more effective than vane lean over a broad frequency spectrum and can be used more efficiently for broadband sound reduction. Results also demonstrate that forward sweep, even though unconventional, might show promise to future sound-reduction mechanisms.

Convergent annular ducts at outflow are efficient sound-reduction mechanisms. The sound reduction is attributed to the reduction of the amplitude of the lower-order propagating modes. These modes attenuate because of the increased spanwise radial phase variation along the stator vanes. However, significant sound downstream sound power increase is possible, if higher-order modes cut on.

Finally, in real fans the vanes are loaded, the flow is viscous, and the upstream mean flow is not uniform and has a swirling motion. These real flow effects modify the vanes acoustic response and can alter some of the conclusions of the present simple model. Nevertheless, the present three-dimensional model by examining the interaction between the incident disturbances and the duct modes gives insightful explanations for the effectiveness of lean, sweep, and duct convergence as means of passive fan noise control. It also provides useful ideas for future research and experimental verification of the results put forth in the present paper.

Acknowledgments

This research was partially supported by the Ohio Aerospace Institute Aeroacoustic Consortium and Office of Naval Research Grant N00014-00-1-0130 and monitored by Ki-Han Kim.

References

[1]Gliebe, P. R., "Aeroacoustics in Turbomachines and Propellers-Future Research Needs," *Unsteady Aerodynamics, Aeroacoustics, and Aeroelasticity of Turbomachines and Propellers*, edited by H. M. Atassi, Springer-Verlag, New York, 1993, pp. 621–642.

[2]Envia, E., "Fan Noise Reduction: An Overview," *International Journal of Aeroacoustics*, Vol. 1, No. 1, 2002, pp. 43–64.

[3]Sutliff, D., Tweedt, D., Fite, E., and Envia, E., "Low Speed Fan Noise Reduction with Trailing Edge Blowing," NASA TM 2002-211559, May 2002.

[4]Tyler, J. M., and Sofrin, T. G., "Axial Flow Compressor Noise Studies," *SAE Transactions*, Vol. 70, 1962, pp. 309–332.

[5]Elliot, D. M., and Dittmar, J. H., "Some Acoustic Results from the Pratt and Whitney Advanced Ducted Propulsor Model," AIAA Paper 2000-0351, Jan. 2000.

[6]McAlpine, A., Wright, M. C. M., Batard, H., and Thezelais, S., "Finite/Boundary Element Assessment of a Turbofan Splice Intake Liner at Supersonic Fan Operating Conditions," AIAA Paper 2003-3305, May 2003.

[7]Groeneweg, J., Sofrin, T., Rice, E., and Gliebe, P., "Turbomachinery Noise," *Aeroacoustics of Flight Vehicles: Theory and Practice. Volume 1: Noise Sources*, edited by H. H. Hubbard, NASA RP-1258, 1991, pp. 151–209.

[8]Elhadidi, B., "Sound Generation and Propagation in Annular Cascades with Swirling Flows," Ph.D. Dissertation, Aerospace and Mechanical Engineering, Univ. of Notre Dame, Notre Dame, IN, Jan. 2002.

[9]Woodward, R. P., Elliott, D. M., Hughes, C. E., and Berton, J. J., "Benefits of Swept and Leaned Stators for Fan Noise Reduction," *Journal of Aircraft*, Vol. 38, No. 6, 2001, pp. 1130–1138.

[10]Envia, E., and Nallasamy, M., "Design Selection and Analysis of a Swept and Leaned Stator Concept," *Journal of Sound and Vibration*, Vol. 228, No. 4, 1999, pp. 793–836.

[11]Heidelberg, L., "Comparison of Tone Mode Measurements For a Forward Swept and Baseline Rotor Fan," AIAA Paper 2003-3293, May 2003.

[12]Schulten, J. B. H. M., "Sound Generated by Rotor Wakes Interacting with a Leaned Vane Stator," *AIAA Journal*, Vol. 20, No. 10, 1982, pp. 1352–1358.

[13]Schulten, J. B. H. M., "Vane Sweep Effects on Rotor/Stator Interaction Noise," *AIAA Journal*, Vol. 35, No. 6, 1997, pp. 945–951.

[14]Goldstein, M. E., "Unsteady Vortical and Entropic Distortions of Potential Flows Round Arbitrary Obstacles," *Journal of Fluid Mechanics*, Vol. 89, 1978, pp. 433–468.

[15]Atassi, H. M., "Unsteady Aerodynamics of Vortical Flows: Early and Recent Developments," *Aerodynamics and Aeroacoustics*, edited by K.-Y. Fung, World Scientific, Singapore, 1994, pp. 121–172.

[16]Golubev, V. V., and Atassi, H. M., "Unsteady Swirling Flows in Annular Cascades. Part II. Aerodynamic Blade Response," *AIAA Journal*, Vol. 38, No. 7, 2000, pp. 1150–1158.

[17]Atassi, H. M., Ali, A. A., Atassi, O. V., and Vinogradov, I. V., "Scattering of Incident Disturbances by an Annular Cascade in a Swirling Flow," *Journal of Fluid Mechanics*, Vol. 499, 2004, pp. 111–138.

[18]McInnes, L., Balay, S., Gropp, W., and Barry, S., "Petsc Users Manual," Argonne National Lab., ANL-95/11-Rev. 2.1.0, Argonne, IL, 2000.

[19]Hanson, D. B., "Fan Stator with Harmonic Excitation by Rotor Wake," *Third Computational Aeroacoustics (CAA) Workshop on Benchmark Problems*, Ohio Aerospace Inst., Cleveland, OH, 1999, Chap. 4.

[20]Schulten, J. B. H. M., and Namba, M., "Numerical Results for Lifting Surface Theory," National Aerospace Lab., NLR, Technical Rept. NLR-TP-2000-013, Noordoostpolder, The Netherlands, Jan. 2000.

[21]Lakshminarayana, B., *Fluid Dynamics and Heat Transfer of Turbomachinery*, Wiley-Interscience, Hoboken, NJ, 1995.

[22]Atassi, H. M., and Hamad, G., "Sound Generation in a Cascade by 3D Disturbance Convected in a Subsonic Flow," AIAA Paper 81-2046, Oct. 1981.

[23]Majumdar, S. J., and Peake, N., "Three-Dimensional Effects in Cascade-Gust Interaction," *Wave Motion*, Vol. 23, No. 4, 1996, pp. 321–337.

[24]Envia, E., "Fan Noise Source Diagnostic Test-Vane Unsteady Pressure Results," AIAA Paper 2002-2430, June 2002.

[25]Atassi, H. M., Dusey, M., and Davis, C. M., "Acoustic Radiation from a Thin Airfoil in Nonuniform Subsonic Flows," *AIAA Journal*, Vol. 31, No. 1, 1993, pp. 12–19.

[26]Sbardella, B. J., Tester, L., and Imregun, M., "A Time-Domain Method for the Prediction of Sound Attenuation in Lined Ducts," *Journal of Sound and Vibration*, Vol. 239, No. 3, 2001, pp. 379–396.

[27]Rienstra, S. W., "Sound Transmission in Slowly Varying Circular and Annular Lined Ducts with Flow," *Journal of Fluid Mechanics*, Vol. 380, 1999, pp. 279–296.

K. Ghia
Associate Editor